Transverse momentum dependence of Ω/ϕ ratio in high energy collisions*

Hai-hong Li (李海宏)[1] Jun Song (宋军)[1] Feng-lan Shao (邵凤兰)[2]

[1]School of Physics and Electronic Engineering, Jining University, Shandong 273155, China
[2]School of Physics and Physical Engineering, Qufu Normal University, Shandong 273165, China

Abstract: We apply a constituent-quark equal-velocity combination model to study the p_T dependence of the Ω/ϕ ratio in pp, p-Pb, and Pb-Pb collisions at LHC energies. We demonstrate that the relative rate of change of the Ω/ϕ ratio is dominated by the curvature property of the p_T spectrum of strange quarks just before hadronization. Using experimental data for ϕ mesons after applying a quark-number scaling procedure, we extract the p_T spectrum of strange quarks just before hadronization and study its curvature property in high- and low-multiplicity events in pp collisions at $\sqrt{s}$ = 7 and 13 TeV, p-Pb collisions at $\sqrt{s_{NN}}$= 5.02 TeV, and Pb-Pb collisions at $\sqrt{s_{NN}}$= 2.76 TeV. We use these curvature properties of the p_T spectra of strange quarks to explain the observed p_T dependence of the Ω/ϕ ratio in these collisions. We discuss the possible origin of the change in the curvature property of the p_T spectra of strange quarks just before hadronization by considering the influence of strong collective flow formed during partonic-stage evolution in collisions at LHC energies.

Keywords: relativistic heavy-ion collisions, hadronization, quark combination mechanism, Large Hadron Collider

DOI: 10.1088/1674-1137/aeb6d4 **CSTR:**

CPC Accepted

I. INTRODUCTION

The baryon-to-meson ratio as a function of transverse momentum (p_T) is a sensitive probe of the hadronization mechanism of final-state parton systems created in high-energy collisions. Measurements of the enhancement of the p/π ratio at RHIC [1, 2] have motivated the application of the quark combination mechanism to describe the hadronization of the hot, dense quark matter created in ultra-relativistic heavy-ion collisions [3−6]. The p/π and Λ/K^0_S ratios are two of the most easily measured baryon/meson ratios; they have been widely reported in pp, pA, and AA collisions at RHIC and LHC energies [2, 7−14] and extensively studied and discussed in various theoretical models of hadron production [3−6, 15−20]. In recent years, baryon/meson ratios in the charm sector, such as Λ^0_c/D^0, have also been measured [21−25], which has shed new light on the hadronization of charm quarks in the low and intermediate p_T range in high-energy collisions [26−31].

Because they involve only strange (anti-)quarks, the production of Ω and ϕ is particularly interesting for revealing the properties of hadron production during the hadronization of soft quark systems created in high-energy collisions. As is well known, strange hadrons have relatively small interaction cross sections with other hadrons and are only weakly affected by hadronic re-scattering [32, 33]. Compared with those for π, protons, and K^0_S, the feed-down corrections for Ω and ϕ are also relatively weak. These advantages make Ω and ϕ clean probes of the hadron production mechanism at the hadronization stage. However, the Ω/ϕ ratio is not often reported in experiments [34, 35], mainly because of the relatively poor statistics for the Ω baryon, and theoretical studies in various popular combination (coalescence) models are also limited [4, 6, 36−38].

In recent years, the LHC has accumulated extensive data on Ω and ϕ in pp, p-Pb, and Pb-Pb collisions, making a meaningful analysis of the Ω/ϕ ratio feasible. To investigate the underlying dynamics of the Ω/ϕ ratio as a function of p_T, we select two collision systems: high-multiplicity pp collisions at $\sqrt{s}$ = 13 TeV and central Pb-Pb collisions at $\sqrt{s_{NN}}$ = 2.76 TeV. In Fig. 1(a), we show the experimental data for the p_T spectra of ϕ and Ω (i.e., $\Omega^- + \bar{\Omega}^+$) for the event class I+II in pp collisions at $\sqrt{s}$ =13 TeV [39, 40] and for 0-10% centrality in Pb-Pb collisions at $\sqrt{s_{NN}}$ =2.76 TeV [41, 42]. The two collision systems differ considerably in system volume, as can be inferred from the charged-particle multiplicity at mid-rapidity, $\langle dN_{ch}/d\eta\rangle = 21.0 \pm 0.25$ for class I+II pp colli-

Received 16 August 2026; Accepted 21 October 2026

* This work is supported by Shandong Provincial Natural Science Foundation (Grants No. ZR2025MS01) and by the National Natural Science Foundation of China under Grants No. 12375074

©2027 Chinese Physical Society and the Institute of High Energy Physics of the Chinese Academy of Sciences and the Institute of Modern Physics of the Chinese Academy of Sciences and IOP Publishing Ltd. All rights, including for text and data mining, AI training, and similar technologies, are reserved.

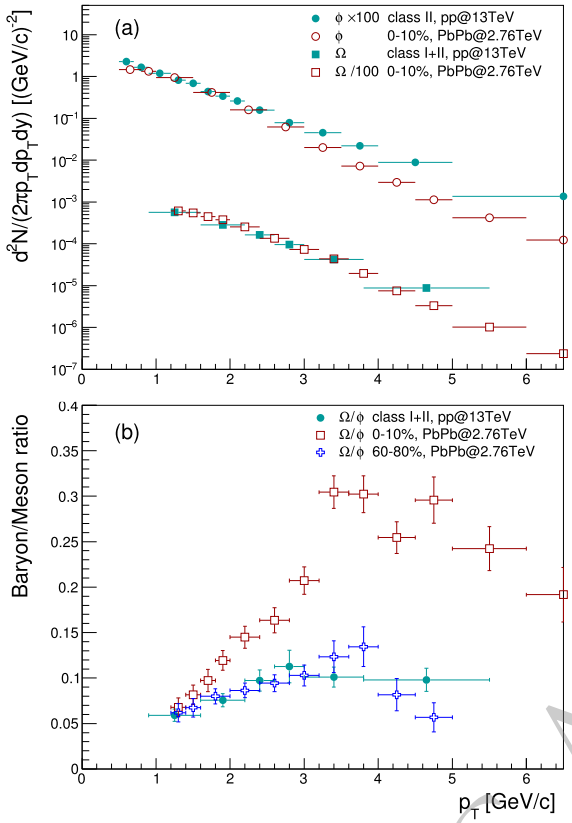


Fig. 1. (color online) (a) p_T spectra of Ω and ϕ in pp collisions at $\sqrt{s}=13$ TeV and in Pb-Pb collisions at $\sqrt{s_{NN}}=2.76$ TeV, and (b) the Ω/ϕ ratio in the two collision systems. Symbols in (a) represent experimental data [39−42], and symbols in (b) represent calculations based on the data.

sions at $\sqrt{s}=13$ TeV [39] and $\langle dN_{ch}/d\eta\rangle = 1446\pm39$ for 0-10% centrality in Pb-Pb collisions at $\sqrt{s_{NN}}=2.76$ TeV [43]. However, Fig. 1(a) shows that, apart from the global normalization (i.e., the yield density at mid-rapidity), the inclusive p_T spectrum of ϕ in pp collisions is similar to that in Pb-Pb collisions in the range $p_T \lesssim 2$ GeV/c but is flatter than the latter at larger p_T. The p_T spectrum of Ω show a similar behavior. The average transverse momentum $\langle p_T\rangle$ for ϕ in pp collisions is 1.456 ± 0.015 GeV/c [39], which is also larger than the value of 1.325 ± 0.028 GeV/c in central Pb-Pb collisions [42]. Using the above data for Ω and ϕ, we evaluate the Ω/ϕ ratio[1)] and show the results in Fig. 1(b). In the low-p_T range, the Ω/ϕ ratio in pp collisions is close to (only slightly smaller than) that in central Pb-Pb collisions, but in the range $2\lesssim p_T\lesssim 5$ GeV/c it is clearly smaller than the latter. In fact, the Ω/ϕ ratio in high-multiplicity pp collisions is quite similar to that in peripheral (60-80% centrality) Pb-Pb collisions at $\sqrt{s_{NN}}=2.76$ TeV. In other words, although we observe flatter p_T spectra of Ω or ϕ in pp collisions, implying relatively more Ω or ϕ at intermediate p_T in pp collisions, the significant enhancement of Ω production relative to ϕ does not occur in high-multiplicity pp collisions.

An interesting question is what underlying dynamics is responsible for such a significant change in the Ω/ϕ ratio from pp collisions to central Pb-Pb collisions at LHC energies. In previous studies of the p/π and Λ/K^0_S ratios, it has usually been argued that the change in the hadron production mechanism from parton fragmentation to quark combination is a sound explanation for such a significant change in baryon/meson ratios at intermediate p_T in small and large collision systems. However, our recent studies show that the quark combination mechanism is also quite effective in explaining the p_T spectra of hadrons in the low and intermediate p_T range in pp collisions at LHC energies [44−46]. One typical piece of evidence is the quark number scaling property of the p_T spectra of Ω and ϕ [44−47]

$$F^{1/3}_{\Omega}(3p_T) = \kappa F^{1/2}_{\phi}(2p_T) \tag{1}$$

where $F(p_T)\equiv dN/dp_T$ and κ is the p_T-independent coefficient. In Fig. 2, we test this scaling property using experimental data for Ω and ϕ at mid-rapidity in different multiplicity classes in pp collisions at $\sqrt{s}=13$ TeV [13, 39−42]. The coefficient κ is chosen to keep the global magnitude of the scaled ϕ data as close as possible to that of Ω and is set to 0.50, 0.57, 0.57, 0.59, 0.59, and 0.65 in multiplicity classes I, II, III+IV, V+VI, VII+VIII, and inel, respectively. Within the current statistics, the scaling property holds well in high-multiplicity events as well as in inelastic events. The scaling property for Pb-Pb collision data at $\sqrt{s_{NN}}=2.76$ TeV was already tested [48]. This scaling property can be understood through the quark equal-velocity combination mechanism via $F_{\Omega}(3p_T)\propto F^3_s(p_T)$ and $F_{\phi}(2p_T)\propto F^2_s(p_T)$, with $F_s(p_T)$ interpreted as the p_T spectra of strange quarks just before hadronization. We therefore argue that the significant change in the Ω/ϕ ratio from pp collisions to central Pb-Pb collisions at LHC energies might not be due to a change in the hadronization mechanism but rather to other dynamics, such as changes in the properties of quark p_T spectra in different collision systems, which is the focus of this paper.

In this paper, we apply a constituent quark equal-velocity combination mechanism to study the production of Ω and ϕ in high-energy pp, p-Pb, and Pb-Pb collisions. We explain the underlying dynamics that influences the p_T dependence of the Ω/ϕ ratio by focusing in particular

1) The p_T binning of the Ω spectra is usually different from that of ϕ. Because the ϕ data points are denser than those of Ω, we first interpolate the ϕ density dN/dp_T at the selected p_T bin of the Ω data and then evaluate the Ω/ϕ ratio. In the interpolation, we use three ϕ data points that completely cover the selected Ω bin and fit these three points with the function $\exp\left[P_2(p_T)\right]$, where $P_2(p_T)$ is a second-order polynomial.

CPC Accepted

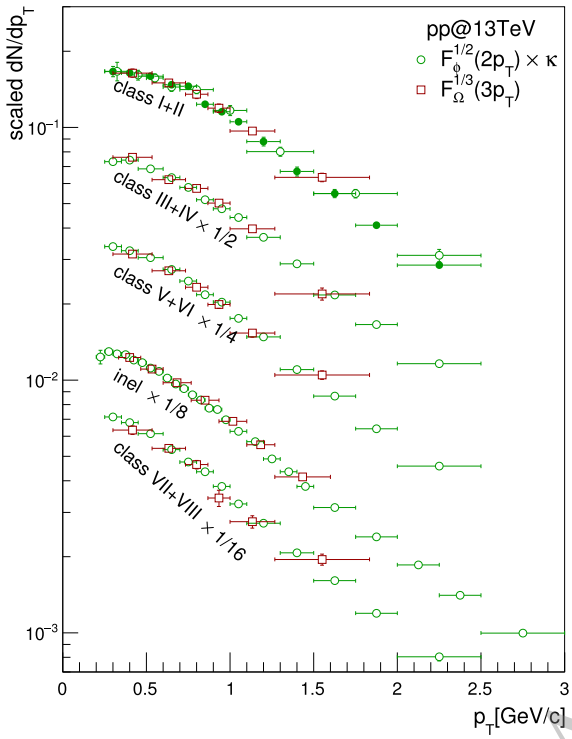


Fig. 2. (color online) The quark number scaling test for the p_T spectra of Ω and ϕ in different multiplicity classes in pp collisions at $\sqrt{s}=13$ TeV is presented. The symbols represent the scaling results obtained from experimental data [13, 39–42]. Since the ϕ data in classes I and II have different p_T bins, the scaling results for the ϕ data in these two classes are shown as open and solid circles, respectively. The results for the other multiplicity classes are multiplied by a factor for clarity.

on the shape of the p_T spectrum of strange quarks just before hadronization. We propose a discrete curvature for the p_T spectrum of strange quarks that can directly determine the rate at which the Ω/ϕ ratio increases or decreases as a function of p_T. We analyze this curvature property of the strange-quark p_T spectra using the scaled ϕ data in pp, p-Pb, and Pb-Pb collisions at LHC energies and use it to explain the Ω/ϕ ratio data in these collisions.

The paper is organized as follows. In Sec. II, we apply the equal-velocity quark combination mechanism to demonstrate how the curvature property of the strange-quark p_T spectrum influences the p_T dependence of the Ω/ϕ ratio. In Sec. III, we discuss the curvature property of the strange-quark p_T spectra obtained from the scaled ϕ data in pp, p-Pb, and Pb-Pb collisions at LHC energies and explain the Ω/ϕ ratio data in these collisions. Section IV presents the summary and discussion.

II. p_T DEPENDENCE OF THE Ω/ϕ RATIO IN EVC MODEL

We apply a specific quark equal-velocity combination (EVC) model [44, 47] to study the p_T dependence of the Ω/ϕ ratio in high-energy collisions. To model the hadronization of the final-state parton system produced in high-energy collisions, we treat constituent quarks and antiquarks as the effective degrees of freedom of the parton system just before hadronization, and assume that hadron formation is mainly characterized by the combination of these constituent quarks and antiquarks with the same velocity. In this framework, the p_T distribution of a hadron ($F(p_T)\equiv dN/dp_T$) is the product of the corresponding distributions of the (anti) quarks

$$F_{B_i}(p_T)=\kappa_{B_i}F_{q_1}(x_1p_T)F_{q_2}(x_2p_T)F_{q_3}(x_3p_T), \tag{2}$$

$$F_{M_i}(p_T)=\kappa_{M_i}F_{q_1}(x_1p_T)F_{\bar{q}_2}(x_2p_T). \tag{3}$$

Here, the momentum fractions satisfy $x_1+x_2+x_3=1$, with $x_i=m_i/(m_1+m_2+m_3)$ $(i=1,2,3)$, for baryon formation, and $x_1+x_2=1$, with $x_i=m_i/(m_1+m_2)$ $(i=1,2)$, for meson formation. m_i is the constituent mass of quark q_i. The coefficients κ_{B_i} and κ_{M_i} are independent of p_T and can be further decomposed and determined by the unitarity of hadronization and several experimental constraints [44, 49].

Applying EVC to Ω^- and ϕ,

$$F_{\Omega^-}(p_T)=\kappa_{\Omega^-}F_s^3(p_T/3), \tag{4}$$

$$F_\phi(p_T)=\kappa_\phi F_s^2(p_T/2). \tag{5}$$

In the LHC case, where the production of Ω^- and $\bar{\Omega}^+$ is almost symmetric, the κ coefficients of Ω (i.e., $\Omega^-+\bar{\Omega}^+$) and ϕ can be written as

$$\kappa_\Omega=\frac{2}{3a}A_{sss}/N_q^2, \tag{6}$$

$$\kappa_\phi=\left(1-\frac{1}{a}\right)A_{ss}C_\phi/N_q. \tag{7}$$

Here, N_q denotes the total number of quarks in the system at hadronization, and $N_q=N_u+N_d+N_s$ when only light-flavor quarks are considered. The parameter a describes the competition between baryon and meson production through the relation $N_M/N_B=3(a-1)$ in the quark combination model. The parameter a is constrained to 4.86 ± 0.14 in our previous studies [50, 51] by reproducing data on proton-antiproton asymmetry in heavy-ion collisions at RHIC and SPS energies and mid-rapidity yields of light-flavor hadrons in p-Pb and Pb-Pb colli-

CPC Accepted

sions at LHC energies. C_ϕ is the conditional probability of forming a ϕ meson from an $s\bar{s}$ pair destined to form a meson. Using the model to reproduce data on the ϕ/K yield ratio in pp, p-Pb and peripheral Pb-Pb collisions at LHC energies [40, 42], C_ϕ is fixed to 0.33 ± 0.02. $A_{ss}^{-1}=2\int dp_T[F_s^{(n)}(p_T)]^2$ and $A_{sss}^{-1}=3\int dp_T[F_s^{(n)}(p_T)]^3$ are determined, respectively, by the integrals of the square and cube of the normalized p_T distribution of strange quarks $F_s^{(n)}(p_T)\equiv F_s(p_T)/N_s$.

The Ω/ϕ ratio in the EVC

$$\frac{F_\Omega(p_T)}{F_\phi(p_T)}=\frac{2\lambda_s}{3C_\phi(a-1)(2+\lambda_s)}\frac{A_{sss}F_s^{(n)}(p_T/3)}{A_{ss}F_s^{(n)}(p_T/2)}. \tag{8}$$

The second fraction on the right-hand side of the equation corresponds to the normalized distributions of Ω and ϕ, which determines the p_T dependence of the Ω/ϕ ratio. The first fraction denotes the global yield ratio of Ω to ϕ. $\lambda_s=N_s/N_u\approx N_s/N_d$ is the factor describing the production suppression of strange quarks relative to up/down quarks, with $N_u\approx N_d$ often assumed in collisions at LHC energies.

To reveal the key ingredient influencing the p_T dependence of the Ω/ϕ ratio, we evaluate

$$\left[\frac{F_\Omega(p_T)}{F_\phi(p_T)}\right]'=\frac{F_\Omega(p_T)}{F_\phi(p_T)}\left[\frac{\partial\ln F_s^{(n)}(\frac{p_T}{3})}{\partial(p_T/3)}-\frac{\partial\ln F_s^{(n)}(\frac{p_T}{2})}{\partial(p_T/2)}\right] \tag{9}$$

and obtain the relative rate of change

$$\left[\ln\frac{F_\Omega(p_T)}{F_\phi(p_T)}\right]'=\left[\frac{\partial\ln F_s^{(n)}(\frac{p_T}{3})}{\partial(p_T/3)}-\frac{\partial\ln F_s^{(n)}(\frac{p_T}{2})}{\partial(p_T/2)}\right]. \tag{10}$$

It depends only on the shape property of the strange quark p_T spectrum. Using the mean-value theorem

$$\frac{\partial\ln F_s^{(n)}(\frac{p_T}{3})}{\partial(p_T/3)}-\frac{\partial\ln F_s^{(n)}(\frac{p_T}{2})}{\partial(p_T/2)}=-\frac{p_T}{6}\left[\ln F_s^{(n)}(\xi)\right]'' \tag{11}$$

where $p_T/3\le\xi\le p_T/2$, we find that the curvature property (convex or concave) of $F_s(p_T)$ is the key factor influencing the p_T dependence of the Ω/ϕ ratio

$$\left[\ln\frac{F_\Omega(p_T)}{F_\phi(p_T)}\right]'=-\frac{p_T}{6}\left[\ln F_s^{(n)}(\xi)\right]''. \tag{12}$$

III. CURVATURE PROPERTY OF p_T SPECTRA OF STRANGE QUARKS AND ITS INFLUENCE ON THE Ω/ϕ RATIO

Given that experimental data for ϕ are usually more abundant than those for Ω, we can extract $F_s(p_T)$ from the experimental data of ϕ

$$F_s(p_T)=\frac{1}{\sqrt{\kappa_\phi}}\left[F_\phi^{(data)}(2p_T)\right]^{1/2}. \tag{13}$$

In Fig. 3(a), we show the scaling results for the experimental p_T spectra of ϕ in high-multiplicity (class II) pp collisions at $\sqrt{s}=13$ TeV and in central Pb-Pb collisions at $\sqrt{s_{NN}}=2.76$ TeV [40, 42]. These results allow us to study the shape of the strange-quark distribution at hadronization. ϕ production in Pb-Pb collisions at LHC energies may contain the contribution of kaon coalescence in hadronic rescattering stage, which can increase v_2 of ϕ and lead to the break of number of constituent-quark scaling for v_2 of ϕ and strange baryons [38, 52, 53] but do not cause the obvious change of p_T spectrum of ϕ [53] and the extracted strange quark distribution.

To evaluate the curvature of the strange-quark p_T spectrum, we fit the discrete data points of $F_s(p_T)$ using the Lévy–Tsallis function [54] and its two variants.

$$\frac{dN^{Levy}}{2\pi p_T dp_T}=N\left[1+\frac{m_T-m}{nC}\right]^{-n}, \tag{14}$$

$$\frac{dN^{Levy-v2}}{2\pi p_T dp_T}=N\left[1+\frac{(m_T-m)^a}{nC}\right]^{-n}, \tag{15}$$

$$\frac{dN^{Levy-v3}}{2\pi p_T dp_T}=N\left[1+\frac{(m_T-m-p_Tv)}{nC\sqrt{1-v^2}}\right]^{-n}. \tag{16}$$

where N, m, n, and C are parameters of the Lévy-Tsallis function, and parameters a and v are introduced into the latter two functions to better tune the shape. The purpose of choosing three fitting functions is to reduce the bias arising from the choice of fitting function. In practical fits, the latter two functions are usually slightly better than the standard Lévy-Tsallis function. The final curvature $\left[\ln F_s(p_T/3)\right]'-\left[\ln F_s(p_T/2)\right]'$ is obtained by averaging the results from the three functions, weighted by the inverse of their fitting-quality values χ^2.

Based on the above fits, we show in Fig. 3(b) the curvature $\left[\ln F_s(p_T/3)\right]'-\left[\ln F_s(p_T/2)\right]'$ for the p_T spectra of strange quarks in high-multiplicity (class II) pp collisions at $\sqrt{s}=13$ TeV and in central Pb-Pb collisions at $\sqrt{s_{NN}}=2.76$ TeV. The curvatures of the strange-quark spectra in both collision systems are positive in the range $p_T\lesssim3$ GeV/c and become negative at larger p_T, which indicates that the Ω/ϕ ratio first increases with p_T, then decreases, and thus exhibits an overall non-monotonic dependence on p_T. Comparing the curvature of the strange-quark spectrum in central Pb-Pb collisions at $\sqrt{s_{NN}}=2.76$ TeV with that in high-multiplicity pp collisions at

CPC Accepted

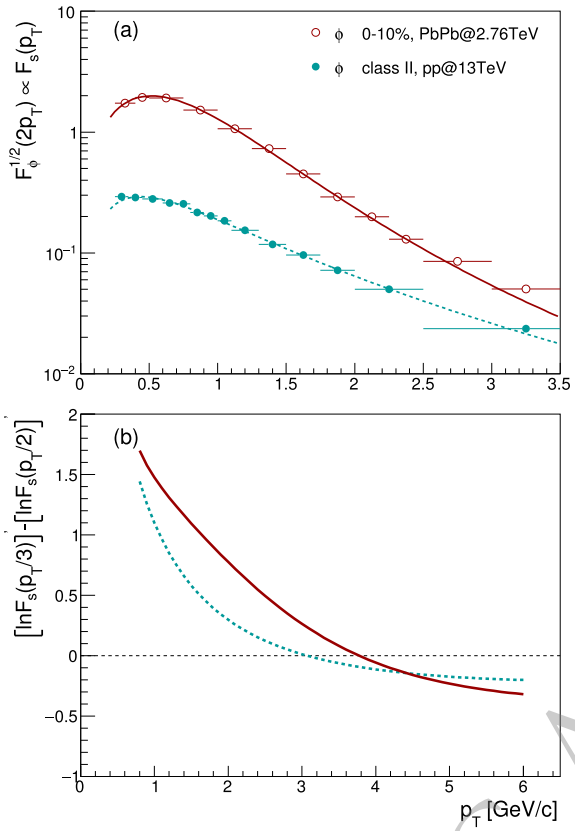


Fig. 3. (color online) (a) The scaled p_T spectra of ϕ in high-multiplicity (class II) pp collisions at $\sqrt{s}$ = 13 TeV and in central Pb-Pb collisions at $\sqrt{s_{NN}}$ = 2.76 TeV. Symbols represent the scaled results from experimental data [40, 42], and lines represent fits using the Lévy-Tsallis function; (b) the curvature $\left[\ln F_s(p_T/3)\right]' - \left[\ln F_s(p_T/2)\right]'$ of the p_T spectra of strange quarks.

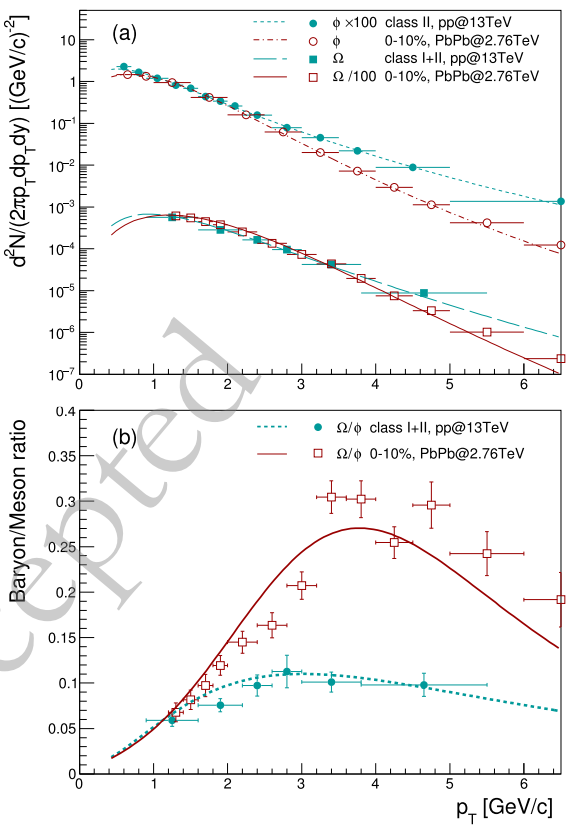


Fig. 4. (color online) (a) p_T spectra of Ω and ϕ in pp collisions at $\sqrt{s}$ = 13 TeV and in Pb-Pb collisions at $\sqrt{s_{NN}}$ = 2.76 TeV and (b) the Ω/ϕ ratio in the two collision systems. The symbols in (a) represent experimental data [39, 40, 41, 42], and those in (b) represent our calculations based on these data. The lines for the p_T spectra of ϕ in (a) are model fits used to fix the p_T spectra of strange quarks just before hadronization, while the other lines are predictions of the EVC model.

CPC Accepted

$\sqrt{s}$ = 13 TeV, we find that the former is clearly higher than the latter in the low p_T range, indicating that the Ω/ϕ ratio in central Pb-Pb collisions increases faster than that in pp collisions. In addition, the p_T position at which the curvature of the strange-quark spectrum vanishes in Pb-Pb collisions is about 0.5 GeV/c larger than that in pp collisions, indicating that the increasing trend of the Ω/ϕ ratio in Pb-Pb collisions can extend to higher p_T.

Using the p_T spectra of strange quarks in Fig. 3(a), which are obtained by fitting ϕ data, we apply the EVC model to calculate the p_T spectrum of Ω and the p_T dependence of the Ω/ϕ ratio in high-multiplicity (class II) pp collisions at $\sqrt{s}$ = 13 TeV and in central Pb-Pb collisions at $\sqrt{s_{NN}}$ = 2.76 TeV. The results are shown in Fig. 4. The ϕ data and our model fits are also shown in Fig. 4(a). In the calculations, $C_\phi = 0.35$ and $a = 4.90$ are used for both collision systems. Because these two parameters affect only the global magnitude of the Ω/ϕ ratio and do not determine its p_T dependence (see Eq. (8)), the effects of their uncertainties, shown below Eq. (7), are not discussed separately in this work. The strangeness suppression factor λ_s is set to 0.32 in pp collisions and 0.42 in Pb-Pb collisions. As expected from the above curvature analysis, the Ω/ϕ ratio in pp collisions increases relatively slowly with p_T, reaches a peak value of about 0.1 at $p_T \approx 3.0$ GeV/c, and then decreases at larger p_T. In central Pb-Pb collisions, owing to the more concave behavior shown in Fig. 3(b), the Ω/ϕ ratio increases rapidly with p_T in the range $p_T \lesssim 3$ GeV/c, reaches a peak value of about 0.25 at $p_T \approx 3.7$ GeV/c, and then decreases at larger p_T.

In Fig. 5, we show a systematic analysis of the Ω/ϕ ratio as a function of p_T in pp collisions at $\sqrt{s}$ = 7 and 13 TeV, p-Pb collisions at $\sqrt{s_{NN}}$ = 5.02 TeV, and Pb-Pb collisions at $\sqrt{s_{NN}}$ = 2.76 TeV. One high-multiplicity and one low-multiplicity event class are selected for each collision system. Panels (a-d) of Fig. 5 show the quark-number-scaling results for the experimental p_T spectra of Ω and ϕ [13, 39–42, 55, 56], from which the shape of the strange-quark distributions just before hadronization can be inferred. The lines are the best fits to these discrete

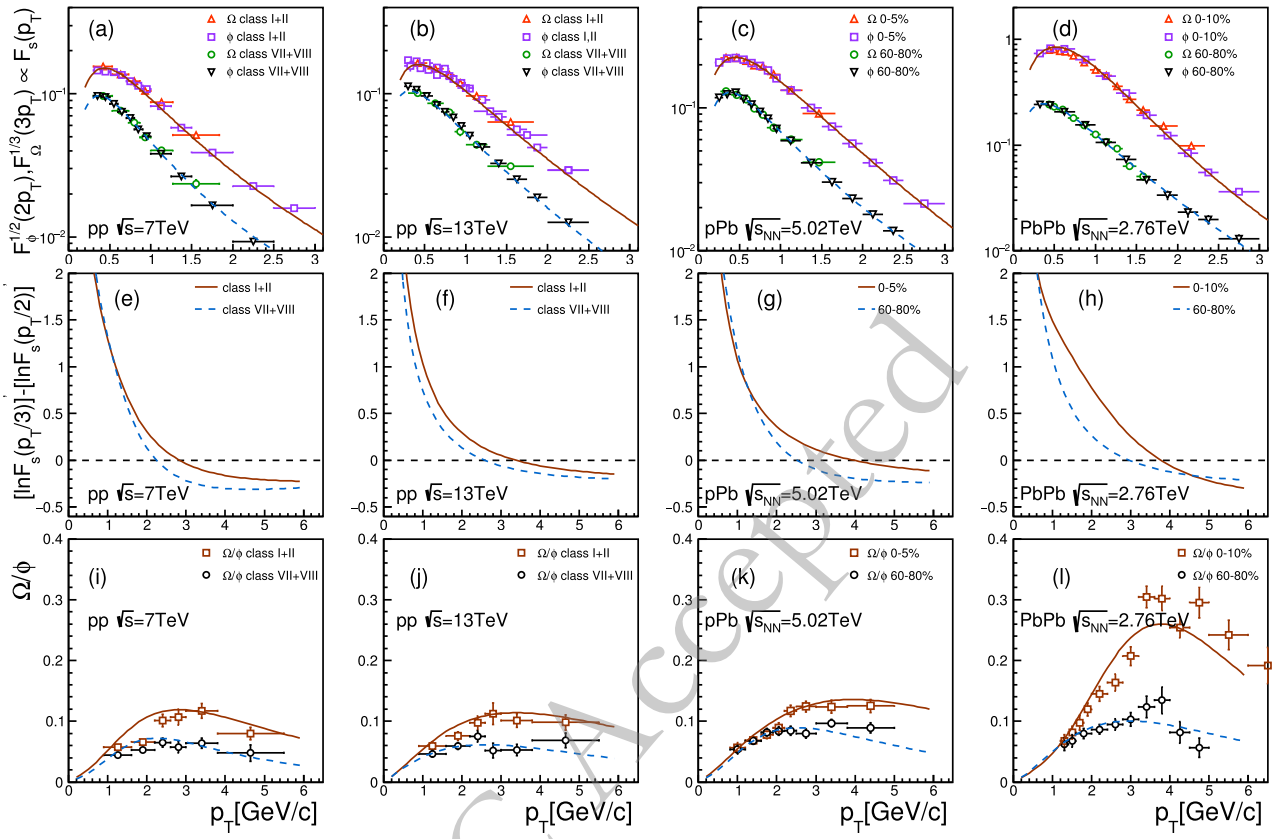


Fig. 5. (color online) (a-d) The quark-number scaling results for experimental data on the p_T spectra of Ω and ϕ in pp, p-Pb, and Pb-Pb collisions at LHC energies [13, 39−42, 55, 56, 61]. The lines are fits to the scaled data; (e-h) the discrete curvature of the p_T distributions of strange quarks calculated from the above fit lines; (i-l) the Ω/ϕ ratios as a function of p_T. Symbols are calculated from the p_T spectra data of Ω and ϕ [13, 39−42, 55, 56, 61]. The lines show model results.

points obtained using Eqs. (14)-(16). Using these smoothed fits, we evaluate the discrete curvature $\left[\ln F_s(p_T/3)\right] - \left[\ln F_s(p_T/2)\right]$ for the p_T distribution of the strange quark and show the results in Fig. 5(e-h). A certain difference is observed between the curvature in the low-multiplicity event class and that in the high-multiplicity event class for each collision system. In particular, the difference between the curvatures in central and peripheral Pb-Pb collisions in panel (h) is relatively larger than the corresponding differences in pp and p-Pb collisions in panels (e-g).

In Fig. 5(i-l), we show the model results for the p_T dependence of Ω/ϕ ratio in the four collision systems. In the evaluation of the Ω/ϕ ratio, the parameters $C_\phi = 0.35$ and $a = 4.90$ are used in all collision systems for simplicity. The strangeness factor λ_s is set to 0.32 (0.29) for high-multiplicity (low-multiplicity) events in pp collisions at $\sqrt{s} = 7$ and 13 TeV, to 0.36 (0.32) for high-multiplicity (low-multiplicity) events in p-Pb collisions at $\sqrt{s_{NN}} = 5.02$ TeV, and to 0.42 (0.33) for central (peripheral) Pb-Pb collisions at $\sqrt{s_{NN}} = 2.76$ TeV. These choices of λ_s for the different collision systems are based on our previous studies [44, 47, 51]. The selected values, such as $\lambda_s = 0.42$ in central AA collisions and $\lambda_s = 0.29$ in low-multiplicity pp collisions, are consistent with calculations of the Wróblewski parameter in the statistical model [57] and in quenched QCD [58], as well as with available experimental measurements [59, 60].

In addition to the suppression of Ω production due to λ_s, Ω production in low-multiplicity events is subject to additional dynamical effects. In low-multiplicity event classes, such as those in pp and p-Pb collisions, the average strange-quark number at midrapidity is very small (less than one for pp collisions) [44, 45]. The formation of Ω in a low-multiplicity event class occurs only in the subset of events containing three or more strange quarks. The Ω yield depends on the fraction of these effective events and therefore on the event-by-event distribution of the strange-quark number at hadronization in this event class. In previous studies [44, 45, 51], we applied a truncated Poisson distribution to study the effect of strange-quark number fluctuations on multistrange baryon production and quantified the resulting suppression of Ω in low-multiplicity event classes. To account for this additional suppression of Ω production in the present study, we introduce an extra suppression factor in front of the

CPC Accepted

normal Ω/ϕ ratio calculated by Eq. (8) for low-multiplicity event classes. Following our previous studies [44, 45, 51], we set it to 0.66 for multiplicity event class VII+VIII in pp collisions at $\sqrt{s}$ = 7 and 13 TeV, and to 0.85 for 60-80% centrality in p-Pb collisions at $\sqrt{s_{NN}}$ = 5.02 TeV and Pb-Pb collisions at $\sqrt{s_{NN}}$ = 2.76 TeV.

We observe several features of the Ω/ϕ ratio in the above four collision systems. Comparing the Ω/ϕ ratios in the low- and high-multiplicity event classes in each collision system shown in Fig. 5(i-l), we see that the peak position of the Ω/ϕ ratio shifts to higher p_T in the high-multiplicity event class. This is also reflected in the curvature of the strange-quark distribution in Fig. 5(e-h). Comparing the Ω/ϕ ratios in the high-multiplicity event class in pp collisions at $\sqrt{s}$ = 7 and 13 TeV with those in p-Pb collisions at $\sqrt{s_{NN}}$ = 5.02 TeV, we observe a weak increase in the Ω/ϕ ratio as the mid-rapidity multiplicity of the systems changes from 21.3 to 45 [55, 56]. However, we observe a strong increase in the Ω/ϕ ratio in central Pb-Pb collisions, which is also reflected in the higher curvature of the strange-quark distribution in the range $p_T < 3$ GeV/c in Fig. 5(h).

Considering the values $\langle p_T\rangle = 1.440 \pm 0.023$, 1.456 ± 0.015 GeV/c for ϕ in the highest-multiplicity pp collisions at $\sqrt{s}$ = 7 and 13 TeV [40, 56], $\langle p_T\rangle = 1.429 \pm 0.008$ GeV/c for central (0-10%) p-Pb collisions at $\sqrt{s_{NN}}$ = 5.02 TeV [55], and $\langle p_T\rangle = 1.325 \pm 0.028$ GeV/c for central Pb-Pb collisions at $\sqrt{s_{NN}}$ = 2.76 TeV [42], we see that the p_T spectra of ϕ (equivalently, strange quarks) in the three small collision systems are overall flatter/broader than those in central Pb-Pb collisions, but this does not lead to the enhancement of Ω production at intermediate p_T. As explained in this work, the curvature of the strange-quark p_T distribution is more relevant to the enhancement of the Ω/ϕ ratios at relatively intermediate p_T. This difference in the curvature of the quark p_T distribution should be related to the difference between the evolution properties of parton systems just before hadronization in small and large systems.

The expansion and evolution of the bulk and hot parton medium produced in relativistic heavy-ion collisions is well modeled by relativistic hydrodynamics, and strong collective flow is established in central collisions [62, 63]. Collective flow has also recently been studied and observed in pp and p-Pb collisions at the LHC [64−66]. Here, we qualitatively demonstrate the influence of strong collective flow on the curvature of the particle p_T spectrum using the fit function in Eq. (16), which is the Lévy-Tsallis function boosted by a radial velocity v. The function has the asymptotic behavior of a thermal distribution as $n \to \infty$. At finite n, the function also behaves like $\exp\left[-(m_T - p_T v - m)/\left(C\sqrt{1-v^2}\right)\right]$ at low p_T, which is the thermal distribution $\exp[-(m_T - m)/C]$ boosted with velocity v. Here, C can be roughly viewed as the temperature in the low-p_T range. At large p_T, the function behaves as a power-law form, $(1 + p_T/a)^{-n}$, whose shape is not influenced by v.

In Fig. 6(a), we show examples of the function in Eq. (16) for three different parameter sets. We choose $v = 0$, $C = 0.3$ as the baseline, which represents a static source with a relatively high temperature (plus the power-law tail from jet physics). We choose $v = 0.6$, $C = 0.3$ as the second example, a high-temperature source with strong collective flow, and $v = 0.6$, $C = 0.164$ as the third example, a low-temperature source with strong collective flow. The third example is intended to capture the expansion and cooling properties of hot-medium evolution; its parameters are chosen so that its $\langle p_T\rangle$ is the same as that of the baseline. The corresponding curvatures of the strange-quark p_T spectrum for these parameter sets are shown in Fig. 6(b). Fig. 6(c) shows the schematic behavior of the Ω/ϕ ratios for the three cases, with the same magnitude set at $p_T = 0.5$ GeV/c, solely to demonstrate the influence of the curvature property of the strange-quark p_T spectrum. The Ω/ϕ ratio in the baseline case (solid line in Fig. 6(c)) increases slowly in the range $p_T \lesssim 3$ GeV/c and then begins to decrease at larger p_T. For the high-temperature, strong-collective-flow case (dashed line), the Ω/ϕ ratio increases rapidly with p_T and then begins to decrease at larger $p_T \gtrsim 5.5$ GeV/c. For the low-temperature, strong-collective-flow case (long-dashed line), the Ω/ϕ ratio increases most rapidly with p_T in the range $p_T \lesssim 3$ GeV/c, can reach a rather high value at p_T of about 3.5 GeV/c, and finally begins to decrease with p_T.

IV. SUMMARY AND DISCUSSION

In this paper, we have applied the constituent quark equal-velocity combination model to study the p_T dependence of the Ω/ϕ ratio in pp, p-Pb, and Pb-Pb collisions at LHC energies. In this model, the p_T distributions of the produced Ω and ϕ are simple products of the p_T spectra of strange quarks just before hadronization. Therefore, we can derive an analytical result for the Ω/ϕ ratio as a function of p_T and identify the key factor influencing the p_T dependence of the Ω/ϕ ratio, i.e., the discrete curvature of the strange quark p_T spectrum. Using the quark number scaling property, we extracted the p_T spectra of strange quarks from the experimental data for ϕ and studied the curvature properties of the strange quark p_T spectra in high- and low-multiplicity events in pp collisions at $\sqrt{s}$ = 7 and 13 TeV, p-Pb collisions at $\sqrt{s_{NN}}$ = 5.02 TeV, and Pb-Pb collisions at $\sqrt{s_{NN}}$ = 2.76 TeV. Finally, using these curvature properties of the strange quark p_T spectra, we successfully explained the observed p_T dependence of the Ω/ϕ ratio in these collisions.

One implication of this work is that the shape property of the quark p_T distribution provides useful informa-

CPC Accepted

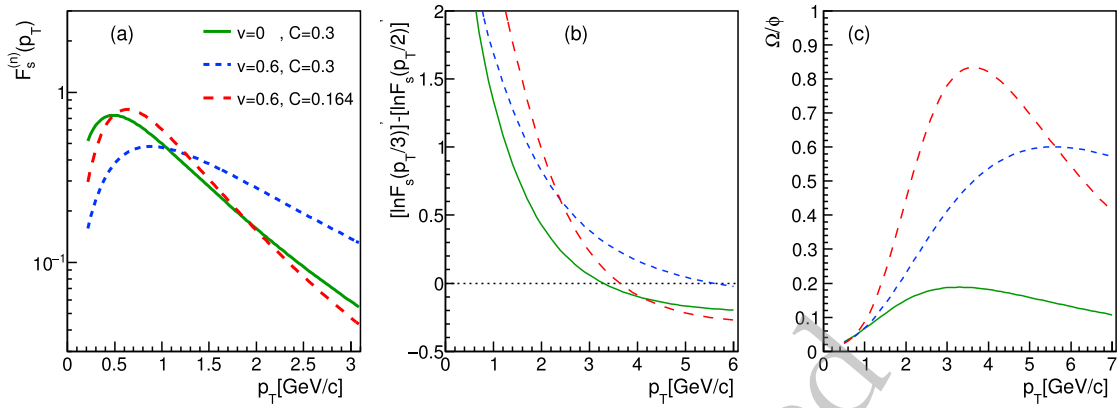


Fig. 6. (color online) (a) The normalized p_T spectrum of strange quarks for different parameter values; (b) the curvature of the spectrum; (c) the schematic behavior of the Ω/ϕ ratio with the same magnitude set at $p_T = 0.5$ GeV/c.

tion for understanding hadron production in high-energy collisions. In this work, we establish a simple connection between the discrete curvature of the strange quark p_T distribution just before hadronization and the p_T dependence of the Ω/ϕ ratio. By comparing the curvature of the strange quark distributions in pp, p-Pb, and Pb-Pb collisions, we find a relatively large change in the curvature of the quark distribution when the collision system changes from pp and p-Pb to Pb-Pb collisions. This large change can be qualitatively understood as a consequence of strong collective flow, such as that formed in central AA collisions.

Similar curvature-property analyses can also be applied to the p_T distributions of hadrons. In our latest work [67], we observed a systematic difference between the curvatures of baryon and meson distributions, which can be explained by the quark combination mechanism at hadronization. In addition, correlations between the characteristic points of the curvature of hadronic p_T distributions and the measured $\langle p_T \rangle$ of hadrons in pp, p-A, and AA collisions suggest an obvious change related to the size (charged-particle multiplicity) of the collision system. This property is also closely connected to the influence of collective flow. In summary, we argue that quantifying the local shape property of particle p_T distributions is a new and effective way to understand particle production in high-energy collisions.

Finally, a comparative discussion on the current work and available studies of Ω/ϕ ratio in other theoretical models and event generators is helpful for readers. According to our previous simulations [45], event generator PYTHIA with the string fragmentation hadronization fails to reproduce the quark number scaling property for p_T spectra of Ω and ϕ shown in Fig. 2 and predicts a relatively small Ω/ϕ ratio in pp collisions at LHC energy which is mainly due to the under prediction of Ω production [39]. EPOS [68] applies a collective hadronization (microcanonical statistical hadronization with an additional longitudinal and radial flow) for central part of collision zone and a parameterization string fragmentation for peripheral part of collision zone. The simulation of EPOS4 [69] in Ref. [70] predicts an increasing Ω/ϕ ratio in range $p_T \lesssim 3.5$ GeV/c in central O+O collisions at $\sqrt{s_{NN}} = 7$ TeV and an increase of Ω/ϕ ratio in range $p_T \lesssim 2$ GeV/c from central to peripheral collisions. Hydrodynamic model of high-energy collisions applies a thermal freeze-out mechanism and predicts a fast increasing Ω/ϕ ratio in low p_T range in Pb-Pb collisions at LHC [36]. Event generator AMPT (string melting version) [71] with a spatial coalescence model for hadronization predicts an increasing Ω/ϕ ratio in range $p_T < 5$ GeV/c with maximum magnitude $\lesssim 0.06$ in central O+O collisions at $\sqrt{s_{NN}} = 7$ TeV according to calculations in [70]. A dynamical quark coalescence model [6] applying the quark information generated by AMPT predicts an increasing Ω/ϕ ratio in range $p_T < 3$ GeV/c with maximum magnitude about 0.7 in central Au+Au collisions at $\sqrt{s_{NN}} = 200$ GeV. A parton recombination model [4] explains the p_T dependence of Ω/ϕ ratio in heavy-ion collisions via the variant contributions of thermal-thermal, thermal-shower and shower-shower components in combination at different p_T. In comparison with these available studies, the current study focuses on the influence of the equal-velocity quark combination hadronization on the p_T dependence of Ω/ϕ ratios in high-energy collisions at LHC energies. p_T distribution of strange quarks just before hadronization is reversely extracted from data of p_T spectrum of ϕ and then is used to calculate Ω spectra and Ω/ϕ ratio. Taking advantage of analytical feature of equal-velocity combination mechanism, the p_T dependence of Ω/ϕ ratio is related to the shape property (i.e., the curvature) of p_T spectrum of strange quarks. The non-monotonic p_T dependence of Ω/ϕ ratio in pp, p-Pb and Pb-Pb collisions at LHC energies was systematically explained via the analysis of the shape property of p_T spectrum of strange quarks in these collisions. In comparison with those avaialable studies, the current study provides a new viewpoint of studying p_T dependence of

CPC Accepted

baryon/meson ratios in high-energy collisions by suggesting the attention to the shape property (e.g., the curvature) of p_T spectra of quarks just before hadronization.

APPENDIX A: FIT PARAMETERS OF THE SCALED p_T SPECTRA OF ϕ

In Table A1, we show parameter values of Eqs. (14)-(16) in fitting the scaled p_T spectra of ϕ in pp, p-Pb and Pb-Pb collisions, which are used to calculate results shown in Figs. 3 and 5. In order to best fit the shape of the scaled ϕ spectra, here we treat m as a free parameter. Parameter v in Eq. (16) is set to be $v \geq 0.02$ in order to show the difference from fittings by Eq. (14).

If we assign a physical mass to m, for example constituent mass $m = 0.5$ GeV of strange quarks just before hadronizaiton, the fitting quality is decreased in general. In Fig. A1 (a), we show the fitting results by Eq. (16) with fixed $m = 0.5$ GeV in Pb-Pb collisions at $\sqrt{s_{NN}} = 2.76$ TeV and compare them with the best fittings with free m setting. We see that χ^2/N_{data} with fixed $m = 0.5$ GeV, the dashed line, is larger than that with free m setting, the solid line, although both are quite close in the figure. In central collisions, we obtain $v = 0.44$ and $C = 0.17$ GeV at fixed $m = 0.5$ GeV, which can be interpreted as an indication of strong collective flow in central Pb-Pb collisions. Therefore, at the end of Sec. 3, we discuss the influence of strong collective flow on the curvature of p_T spectra of strange quarks and the resulting Ω/ϕ ratio in central Pb-Pb collisions at LHC. In peripheral Pb-Pb collisions at $\sqrt{s_{NN}} = 2.76$ TeV, high-multiplicity class II in pp at $\sqrt{s} = 7, 13$ TeV and high-multiplicity 0-5% centrality class in p-Pb collisions at $\sqrt{s_{NN}} = 5.02$ TeV, fitting results by Eq. (16) with fixed $m = 0.5$ GeV, as shown in Fig. A1 (a-c), do not show a tendency to obvious v.

Table A1. Parameter values of Eqs. (14)–(16) used in fitting the scaled p_T spectra of ϕ in pp, p-Pb, and Pb-Pb collisions.

system	Eq. (14)			Eq. (15)				Eq. (16)			
	n	m	C	a	n	m	C	v	n	m	C
pp $\sqrt{s}$ =13TeV class II	4.813	0.318	0.305	0.592	5.776	2.412	0.144	0.024	4.826	0.310	0.299
pp $\sqrt{s}$ =13TeV class VII	5.430	0.050	0.264	0.733	18.49	0.050	0.279	0.020	5.429	0.050	0.259
pp $\sqrt{s}$ =7TeV class II	4.419	0.440	0.265	0.691	4.547	1.895	0.140	0.020	4.437	0.430	0.262
pp $\sqrt{s}$ =7TeV class VII	3.505	0.520	0.184	0.781	2.954	2.078	0.081	0.020	3.526	0.504	0.182
p-Pb $\sqrt{s_{NN}}$ =5.02TeV 0-5%	7.983	0.200	0.374	0.903	13.63	0.200	0.382	0.031	9.447	0.020	0.377
p-Pb $\sqrt{s_{NN}}$ =5.02TeV 60-80%	4.504	0.333	0.248	1.243	3.270	0.158	0.256	0.020	4.512	0.327	0.244
Pb-Pb $\sqrt{s_{NN}}$ =2.76TeV 0-10%	6.314	1.008	0.218	0.910	4.700	2.217	0.121	0.021	4.192	1.507	0.144
Pb-Pb $\sqrt{s_{NN}}$ =2.76TeV 60-80%	6.992	0.230	0.284	0.582	7.928	2.347	0.130	0.020	7.000	0.226	0.279

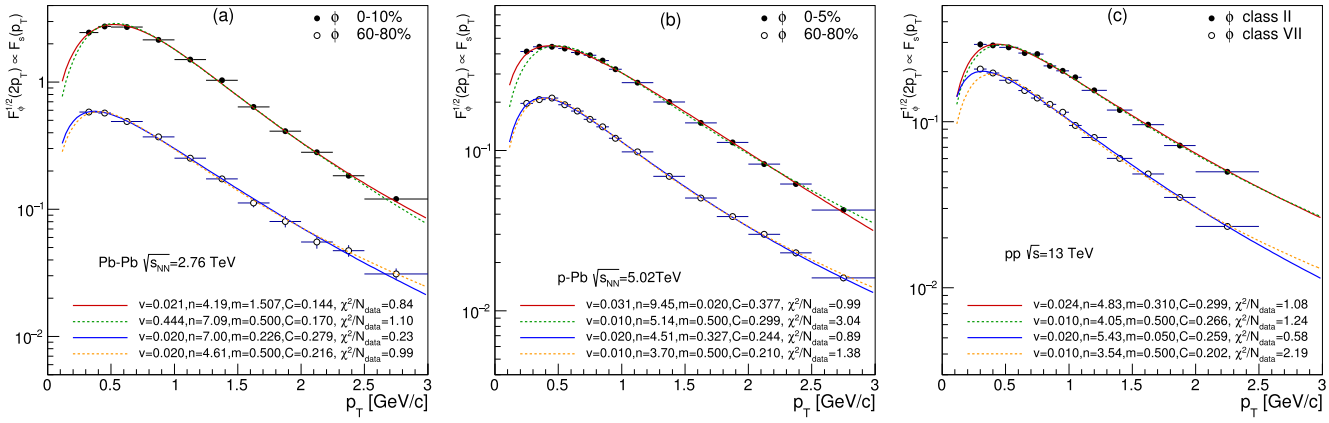


Fig. A1. (color online) The scaled p_T spectra of ϕ in Pb-Pb collisions at $\sqrt{s_{NN}} = 2.76$ TeV (a), p-Pb collisions at $\sqrt{s_{NN}} = 5.02$ TeV (b), and pp collisions at $\sqrt{s} = 13$ TeV (c), together with their corresponding function fits. The symbols represent scaled ϕ data [40, 42, 55], and the lines show the fit results from Eq. (16).

CPC Accepted

References

[1] K. Adcox *et al.* (PHENIX), Phys. Rev. Lett. **88**, 242301 (2002), arXiv: nucl-ex/0112006
[2] B. I. Abelev *et al.* (STAR), Phys. Rev. Lett. **97**, 152301 (2006), arXiv: nucl-ex/0606003
[3] R. C. Hwa and C. B. Yang, Phys. Rev. C **67**, 034902 (2003), arXiv: nucl-th/0211010
[4] R. C. Hwa and C. B. Yang, Phys. Rev. C **75**, 054904 (2007), arXiv: nucl-th/0602024
[5] V. Greco, C. M. Ko, and P. Levai, Phys. Rev. Lett. **90**, 202302 (2003), arXiv: nucl-th/0301093
[6] L.-W. Chen and C. M. Ko, Phys. Rev. C **73**, 044903 (2006), arXiv: nucl-th/0602025
[7] B. I. Abelev *et al.* (STAR), Phys. Rev. C **75**, 064901 (2007), arXiv: nucl-ex/0607033
[8] B. B. Abelev *et al.* (ALICE), Phys. Rev. Lett. **111**, 222301 (2013), arXiv: 1307.5530[nucl-ex]
[9] J. Adam *et al.* (ALICE), Phys. Lett. B **760**, 720 (2016), arXiv: 1601.03658[nucl-ex]
[10] B. B. Abelev *et al.* (ALICE), Phys. Lett. B **736**, 196 (2014), arXiv: 1401.1250[nucl-ex]
[11] B. B. Abelev *et al.* (ALICE), Phys. Lett. B **728**, 25 (2014), arXiv: 1307.6796[nucl-ex]
[12] J. Adams *et al.* (STAR, STAR RICH), (2006), arXiv:nucl-ex/0601042.
[13] S. Acharya *et al.* (ALICE), Eur. Phys. J. C **81**, 256 (2021), arXiv: 2005.11120[nucl-ex]
[14] J. Adam *et al.* (STAR), Phys. Rev. C **102**, 034909 (2020), arXiv: 1906.03732[nucl-ex]
[15] K. Werner, Phys. Rev. Lett. **109**, 102301 (2012), arXiv: 1204.1394[nucl-th]
[16] T. Pierog, I. Karpenko, J. M. Katzy, E. Yatsenko, and K. Werner, Phys. Rev. C **92**, 034906 (2015), arXiv: 1306.0121[hep-ph]
[17] V. Begun, W. Florkowski, and M. Rybczynski, Phys. Rev. C **90**, 054912 (2014), arXiv: 1405.7252[hep-ph]
[18] V. Minissale, F. Scardina, and V. Greco, Phys. Rev. C **92**, 054904 (2015), arXiv: 1502.06213[nucl-th]
[19] C. Bierlich and J. R. Christiansen, Phys. Rev. D **92**, 094010 (2015), arXiv: 1507.02091[hep-ph]
[20] A. Sengupta *et al.* (JETSCAPE), (2025), arXiv:2501.16482[hep-ph].
[21] S. Acharya *et al.* (ALICE), JHEP **04**, 108 (2018), arXiv: 1712.09581[nucl-ex]
[22] R. Aaij *et al.* (LHCb), JHEP **02**, 102 (2019), arXiv: 1809.01404[hep-ex]
[23] R. Aaij *et al.* (LHCb), JHEP 06, 132 (2023), [Erratum: JHEP 05, 021 (2024)], arXiv:2210.06939[hep-ex].
[24] S. Acharya *et al.* (ALICE), Phys. Rev. C **107**, 064901 (2023), arXiv: 2211.14032[nucl-ex]
[25] A. Tumasyan *et al.* (CMS), JHEP **01**, 128 (2024), arXiv: 2307.11186[nucl-ex]
[26] S. Cho, K.-J. Sun, C. M. Ko, S. H. Lee, and Y. Oh, Phys. Rev. C **101**, 024909 (2020), arXiv: 1905.09774[nucl-th]
[27] V. Minissale, S. Plumari, and V. Greco, Phys. Lett. B **821**, 136622 (2021), arXiv: 2012.12001[hep-ph]
[28] J. Song, H.-h. Li, and F.-l. Shao, Eur. Phys. J. C **83**, 852 (2023), arXiv: 2304.00434[hep-ph]
[29] J. Zhao *et al.*, Phys. Rev. C **109**, 054912 (2024), arXiv: 2311.10621[hep-ph]
[30] J. Altmann, A. Dubla, V. Greco, A. Rossi, and P. Skands, Eur. Phys. J. C **85**, 16 (2025), arXiv: 2405.19137[hep-ph]
[31] W.-b. Chang, R.-q. Wang, J. Song, F.-l. Shao, Q. Wang, and Z.-t. Liang, Symmetry **15**, 400 (2023), arXiv: 2302.07546[nucl-th]
[32] A. Shor, Phys. Rev. Lett. **54**, 1122 (1985)
[33] H. van Hecke, H. Sorge, and N. Xu, Phys. Rev. Lett. **81**, 5764 (1998), arXiv: nucl-th/9804035
[34] B. I. Abelev *et al.* (STAR), Phys. Rev. C **79**, 064903 (2009), arXiv: 0809.4737[nucl-ex]
[35] B. B. Abelev *et al.* (ALICE), Phys. Rev. C **91**, 024609 (2015), arXiv: 1404.0495[nucl-ex]
[36] N. Armesto, N. Borghini, S. Jeon, and U. A. Wiedemann, eds., Proceedings, Workshop on Heavy Ion Collisions at the LHC: Last Call for Predictions: Geneva, Switzerland, May 14 - June 8, 2007, Vol. 35 (2008) arXiv:0711.0974[hep-ph].
[37] X.-H. Jin, J.-H. Chen, Y.-G. Ma, S. Zhang, C.-J. Zhang, and C. Zhong, Nucl. Sci. Tech. **29**, 54 (2018)
[38] J. Pu, K.-J. Sun, and L.-W. Chen, Phys. Rev. C **98**, 064905 (2018), arXiv: 1808.04053[nucl-th]
[39] S. Acharya *et al.* (ALICE), Eur. Phys. J. C **80**, 167 (2020), arXiv: 1908.01861[nucl-ex]
[40] S. Acharya *et al.* (ALICE), Phys. Lett. B **807**, 135501 (2020), arXiv: 1910.14397[nucl-ex]
[41] B. B. Abelev *et al.* (ALICE), Phys. Lett. B 728, 216 (2014), [Erratum: Phys.Lett.B 734, 409–410 (2014)], arXiv:1307.5543[nucl-ex].
[42] J. Adam *et al.* (ALICE), Phys. Rev. C **95**, 064606 (2017), arXiv: 1702.00555[nucl-ex]
[43] K. Aamodt *et al.* (ALICE), Phys. Rev. Lett. **106**, 032301 (2011), arXiv: 1012.1657[nucl-ex]
[44] X.-r. Gou, F.-l. Shao, R.-q. Wang, H.-h. Li, and J. Song, Phys. Rev. D **96**, 094010 (2017), arXiv: 1707.06906[hepph]
[45] J.-w. Zhang, H.-h. Li, F.-l. Shao, and J. Song, Chin. Phys. C **44**, 014101 (2020), arXiv: 1811.00975[hep-ph]
[46] H.-h. Li, F.-l. Shao, and J. Song, Chin. Phys. C **45**, 113105 (2021), arXiv: 2103.14900[hep-ph]
[47] J. Song, X.-r. Gou, F.-l. Shao, and Z.-T. Liang, Phys. Lett. B **774**, 516 (2017), arXiv: 1707.03949[hep-ph]
[48] J. Song, F.-l. Shao, and Z.-t. Liang, Phys. Rev. C **102**, 014911 (2020), arXiv: 1911.01152[nucl-th]
[49] J. Song, X.-F. Wang, H.-H. Li, R.-Q. Wang, and F.-L. Shao, Phys. Rev. C **103**, 034907 (2021), arXiv: 2007.14588[nucl-th]
[50] J. Song and F.-l. Shao, Phys. Rev. C **88**, 027901 (2013), arXiv: 1303.1231[nucl-th]
[51] F.-l. Shao, G.-j. Wang, R.-q. Wang, H.-h. Li, and J. Song, Phys. Rev. C **95**, 064911 (2017), arXiv: 1703.05862[hepph]
[52] B. B. Abelev *et al.* (ALICE), JHEP **06**, 190 (2015), arXiv: 1405.4632[nucl-ex]
[53] J. Song, H.-h. Li, and F.-l. Shao, Eur. Phys. J. C **81**, 5 (2021), arXiv: 2008.03017[nucl-th]
[54] C. Tsallis, J. Statist. Phys. **52**, 479 (1988)
[55] J. Adam *et al.* (ALICE), Eur. Phys. J. C **76**, 245 (2016), arXiv: 1601.07868[nucl-ex]
[56] S. Acharya *et al.*, Phys. Rev. C **99**, 024906 (2019), arXiv: 1807.11321[nucl-ex]
[57] F. Becattini, M. Gazdzicki, and J. Sollfrank, Eur. Phys. J. C **5**, 143 (1998), arXiv: hep-ph/9710529
[58] R. V. Gavai and S. Gupta, Eur. Phys. J. C **43**, 31 (2005), arXiv: hep-ph/0502198
[59] G. Bocquet *et al.*, Phys. Lett. B **366**, 447 (1996)
[60] M. Mestayer *et al.* (CLAS), Phys. Rev. Lett. **113**, 152004 (2014), arXiv: 1412.0974[nucl-ex]
[61] J. Adam *et al.* (ALICE), Phys. Lett. B **758**, 389 (2016),

CPC Accepted

arXiv: 1512.07227[nucl-ex]
[62] P. F. Kolb and U. W. Heinz, "Hydrodynamic description of ultrarelativistic heavy ion collisions, " in Quark–Gluon Plasma 3, edited by R. C. Hwa and X.-N. Wang (WORLD SCIENTIFIC, 2003) pp. 634–714, arXiv:nucl-th/0305084.
[63] C. Gale, S. Jeon, and B. Schenke, Int. J. Mod. Phys. A **28**, 1340011 (2013), arXiv: 1301.5893[nucl-th]
[64] W. Zhao, Y. Zhou, H. Xu, W. Deng, and H. Song, Phys. Lett. B **780**, 495 (2018), arXiv: 1801.00271[nucl-th]
[65] W. Zhao, C. M. Ko, Y.-X. Liu, G.-Y. Qin, and H. Song, Phys. Rev. Lett. **125**, 072301 (2020), arXiv: 1911.00826[nucl-th]
[66] S. Acharya *et al*. (ALICE), Nature Commun. **17**, 2585 (2026), arXiv: 2411.09323[nucl-ex]
[67] J. Song, H.-h. Li, and F.-l. Shao, Phys. Rev. D **112**, 114025 (2025), arXiv: 2512.15178[hep-ph]
[68] K. Werner, F.-M. Liu, and T. Pierog, Phys. Rev. C **74**, 044902 (2006), arXiv: hep-ph/0506232
[69] K. Werner, Phys. Rev. C **109**, 014910 (2024), arXiv: 2306.10277[hep-ph]
[70] M. U. Ashraf, A. M. Khan, J. Singh, G. Nigmatkulov, H. Roch, and S. Kabana, Chin. J. Phys. **98**, 768 (2025), arXiv: 2406.04096[hep-ph]
[71] Z.-W. Lin, C. M. Ko, B.-A. Li, B. Zhang, and S. Pal, Phys. Rev. C **72**, 064901 (2005), arXiv: nucl-th/0411110

CPC Accepted